ACS chemical biology

Articles

pubs.acs.org/acschemicalbiology

Probing the Ca^{2+} Switch of the Neuronal Ca^{2+} Sensor GCAP2 by Time-Resolved Fluorescence Spectroscopy

Heiko Kollmann,[†] Simon F. Becker,[†] Javid Shirdel,[†] Alexander Scholten,[§] Anna Ostendorp,[§] Christoph Lienau,[†,‡] and Karl-Wilhelm Koch*[,§,‡,∥]

[†]Ultrafast Nano-Optics, Institute of Physics and [§]Biochemistry, Institute of Biology and Environmental Sciences, Faculty V, University of Oldenburg, D-26111 Oldenburg, Germany

[‡]Center of Interface Science and [∥]Research Center Neurosensory Science, University of Oldenburg, D-26111 Oldenburg, Germany

ABSTRACT: We report fluorescence lifetime and rotational anisotropy measurements of the fluorescent dye Alexa647 attached to the guanylate cyclase-activating protein 2 (GCAP2), an intracellular myristoylated calcium sensor protein operating in photoreceptor cells. By linking the dye to different protein regions critical for monitoring calcium-induced conformational changes, we could measure fluorescence lifetimes and rotational correlation times as a function of myristoylation, calcium, and position of the attached dye, while GCAP2 was still able to regulate guanylate cyclase in a Ca^{2+}-sensitive manner. We observe distinct site-specific variations in the fluorescence dynamics when externally changing the protein conformation. A clear reduction in fluorescence lifetime suggests that in the calcium-free state a dye marker in amino acid position 131 senses a more hydrophobic protein environment than in position 111. Saturating GCAP2 with calcium increases the fluorescence lifetime and hence leads to larger exposure of position 111 to the solvent and at the same time to a movement of position 131 into a hydrophobic protein cleft. In addition, we find distinct, biexponential anisotropy decays reflecting the reorientational motion of the fluorophore dipole and the dye/protein complex, respectively. Our experimental data are well described by a "wobbling-in-a-cone" model and reveal that for dye markers in position 111 of the GCAP2 protein both addition of calcium and myristoylation results in a pronounced increase in orientational flexibility of the fluorophore. Our results provide evidence that the up-and-down movement of an α-helix that is situated between position 111 and 131 is a key feature of the dynamics of the protein−dye complex. Operation of this piston-like movement is triggered by the intracellular messenger calcium.

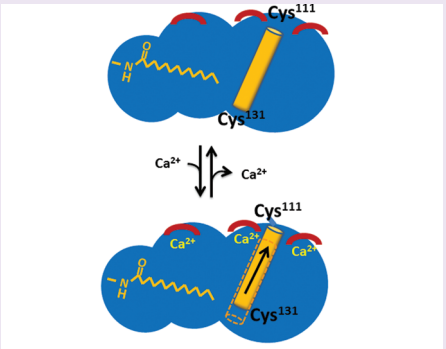

Piston-like movement of an α-helical segment in the calcium sensor GCAP2

Signal transduction in neurosensory cells requires the precise operation of interacting proteins to achieve physiological responses on short time intervals. Photoreceptor cells for example are exquisite light detectors that respond to photons on a millisecond time scale.[1,2] The extraordinary efficiency of rod and cone photoreceptor cells to detect single photons and to adjust to ambient light conditions that can change by up to 10 orders of magnitude relies on the well balanced interplay of two second messengers, cGMP and calcium.[1−3] Illumination leads to a decrease of cGMP *via* a G protein-mediated signaling cascade within a few hundred milliseconds.[1−4] The cytoplasmic concentration of cGMP finally controls the gating of a cyclic nucleotide-gated (CNG) channel in the photoreceptor cell plasma membrane.[5] Decrease of cGMP by light leads to closure of CNG-gated channels and prevents Ca^{2+} from entering the cell. In consequence the cytoplasmic Ca^{2+} concentration ($[Ca^{2+}]$) also decreases, because a $Na^+/Ca^{2+},K^+$-exchanger is transporting Ca^{2+} from the cytoplasmic site into the extracellular medium.[6] Ca^{2+}-dependent feedback loops respond to changes in cytoplasmic Ca^{2+} and thereby regulate several biochemical steps within 100 ms after start of illumination.[1−4] Key neuronal Ca^{2+}-sensor proteins involved in these feedback loops in vertebrate rod and cone cells are recoverin and guanylate cyclase-activating proteins (GCAPs).[7−11] Recoverin[7] inhibits the activity of rhodopsin kinase, when it has two Ca^{2+} bound relieving this inhibition, when $[Ca^{2+}]$ decreases after illumination. GCAPs control the activity of membrane-bound sensory guanylate cyclases (ROS-GC 1 and 2) mainly by increasing the cyclase activity below a free $[Ca^{2+}]$ of 0.5 μM.[8−11] Mammalian GCAPs and recoverin are posttranslationally acylated (mainly myristoylated) at the N-terminus leading to a further diversification of their molecular properties.[7−11] In recoverin the myristoyl group is exposed when Ca^{2+} is bound and is buried inside a hydrophobic cavity of the Ca^{2+}-free state.[12,13] It further controls allosterically the Ca^{2+}-induced conformational transition in recoverin,[14,15] which can be monitored by a fluorescent dye Alexa647 attached to recoverin's unique cysteine.[16] In contrast, GCAPs do not perform such a Ca^{2+}-myristoyl switch.[17,18] Instead the crystal structure of Ca^{2+}-GCAP1 shows that the myristoyl chain is buried in a hydrophobic pocket leading to a general stabilization of the protein structure.[19,20] Recent ^2H NMR

Received: November 17, 2011
Accepted: March 12, 2012
Published: March 12, 2012

studies on deuterated myristoylated GCAP2, however, showed that the myristoyl group of GCAP2 is inserted into lipid membranes both in the presence and absence of Ca^{2+}, whereas nonmyristoylated GCAP2 binds to membranes with almost the same affinity.[21,22]

These structural results indicate that the myristoyl group influences the properties of different GCAP isoforms in different ways, for example, by controlling the catalytic efficiency of the target guanylate cyclase ROS-GC1 differently.[23]

Another crucial property of GCAPs is to undergo conformational changes that are triggered by Ca^{2+}. For the mammalian isoforms GCAP1 and GCAP2 these changes have been investigated by gel shift assays and limited tryptic digestions,[24−26] intrinsic tryptophan fluorescence emission,[26,27] CD spectroscopy,[24] and by testing the reactivity of endogenous cysteines.[28−30] The activation process is even more complex taking into account that Ca^{2+} is exchanged for Mg^{2+} in the Ca^{2+}-binding sites (EF-hands) of GCAP1 and 2.[31,32] From all of these studies it is clear that both the presence of the myristoyl group and the calcium concentration strongly influence the structure and function of GCAP proteins, but details of how they influence the local protein conformation and its dynamics are to a large extent not understood.

A powerful strategy for probing such influences is the site-specific labeling of a protein with appropriate dye markers, probing the local protein environment, *e.g.*, *via* its effect on the fluorescence dynamics of the dye molecule. A previous study indicated that the three endogenous cysteine residues in GCAP2 are sensitive to Ca^{2+}-induced conformational changes and therefore might move upon a Ca^{2+} trigger.[30] It was the aim of the present study to test this hypothesis by site-specific labeling with the fluorescence marker Alexa647 and employing fluorescence lifetime and anisotropy measurements on a nanosecond time scale. Photophysical properties as fluorescence lifetimes and rotational reorientation times clearly correlated with the myristoylation and Ca^{2+}-bound state of the investigated GCAP2 conjugates. Our observations are well accounted for by a qualitative "wobbling-in-a-cone" model for the dynamics of the dye-protein complex giving new insight into the conformational dynamics of this class of calcium sensors.

RESULTS AND DISCUSSION

In order to probe Ca^{2+}-induced conformational changes in specific regions of the GCAP2 protein, we adopted a site-specific labeling strategy and exchanged two of the cysteine (C) residues in GCAP2[10] against alanine (A), resulting in three different mutants, CAA, ACA, and AAC (see Methods). This exchange does not disturb the general functionality of the protein. The modified GCAP2 is still able to undergo Ca^{2+}-induced conformational changes and can activate its target membrane-bound guanylate cyclase in a Ca^{2+}-dependent manner.[30,33] It is important, moreover, that all cysteines are accessible by the thiol-modifying reagent DTNB,[30] even though cysteine residues in position 35 and 111 are slightly less reactive in the presence of Ca^{2+}. This offers a viable route to introduce a fluorescent dye such as Alexa647 linking the maleimide reactive group of the dye to freely accessible cysteine groups. Here, we adopted this strategy, labeling all three GCAP2 mutants with Alexa647 to probe Ca^{2+}-induced conformational changes *via* the fluorescence dynamics of the dye marker. Initial fluorescence lifetime measurements of the dye-labeled mutant CAA showed no difference in the decaying fluorescence signal in the presence or absence of Ca^{2+}. Thus, we focused our studies on the mutants ACA and AAC.

Biochemical Properties of GCAP2 Mutants Labeled with Alexa647. A critical prerequisite for our fluorescence studies was to ensure that the labeled proteins could still undergo Ca^{2+}-induced conformational changes and maintain their biological function. To meet this requirement, all mutants were overexpressed in *E. coli* and were prepared from *E. coli* extracts by chromatographic procedures to apparent homogeneity. GCAP2 forms were myristoylated by the activity of a co-expressed yeast *N*-myristoyl-transferase. The degree of myristoylation was 92% and 89% for the ACA and AAC mutants, respectively, as determined by a reversed phase HPLC analysis (Table 1). The labeling was successful for all GCAP2 mutants with stoichiometric ratios of dye per protein of nearly 1:1 for almost all GCAP2 forms (Table 1). A lower degree of labeling (0.64:1) was only observed for myristoylated AAC, which is consistent with our previous observation that cysteine at position 111 has a slightly restricted accessibility for thiol-modifying reagents.[30]

Table 1. Labeling of GCAP2 with Alexa647

sample	degree of myristoylation (%)	labeled (%)	unlabeled (%)
nmyr ACA		92.6	7.4
myr ACA	92	90.9	9.1
nmyr AAC		92.1	7.9
myr AAC	89	64.0	36.0

It is known that GCAPs, like other neuronal Ca^{2+}-sensor proteins, exhibit a change in their electrophoretic mobility when they are loaded with Ca^{2+}, which is seen as a Ca^{2+} shift in a polyacrylamide gel electrophoresis (PAGE) analysis and serves as a qualitative indicator of Ca^{2+}-induced conformational changes.[8−11,24−26] This shift is visible for all labeled GCAP2 mutants (Figure 1a). These results demonstrate that dye-labeled cysteine mutants of GCAP2 undergo Ca^{2+}-induced conformational changes. Presence of $MgCl_2$ enhances the shift indicating also that GCAP2 mutants bind Mg^{2+}, which is consistent with the observation that mammalian GCAP1 and GCAP2 are Ca^{2+}/Mg^{2+}-binding proteins.[31,32]

GCAP2 is a regulator of membrane bound ROS-GCs in mammalian photoreceptor cells.[10,17,23,30,33] In order to test whether labeled GCAP2 mutants were able to stimulate ROS-GC activities at low free $[Ca^{2+}]$ (<10 nM), we measured the GC activities at high (33 μM) and low (3 nM) $[Ca^{2+}]$. All mutants activated native ROS-GCs in photoreceptor rod outer segment membrane preparations. The *x*-fold activation was 64−74% of the control values obtained with the wildtype (data not shown), in agreement with our previously published data that the mutation did not disturb the structural and functional properties of GCAP2.[30,33] Introduction of the dye Alexa647 into the site of the remaining cysteine did not disturb the stimulatory activity of GCAP2 in general, but the attachment of the dye lowered the extent of GCAP2-dependent ROS-GC activity at low free $[Ca^{2+}]$. The remaining stimulatory activity was for each mutant as follows (percentage of *x*-fold activation in comparison to the nonlabeled form): nonmyristoylated ACA (90%), myristoylated ACA (76%), nonmyristoylated AAC (75%), and myristoylated AAC (82%) (Figure 1b). Finally, the Ca^{2+}-sensitive activation profile of ROS-GC activity remained essentially the same for the labeled and the nonlabeled protein,

dx.doi.org/10.1021/cb3000748 | *ACS Chem. Biol.* 2012, 7, 1006−1014

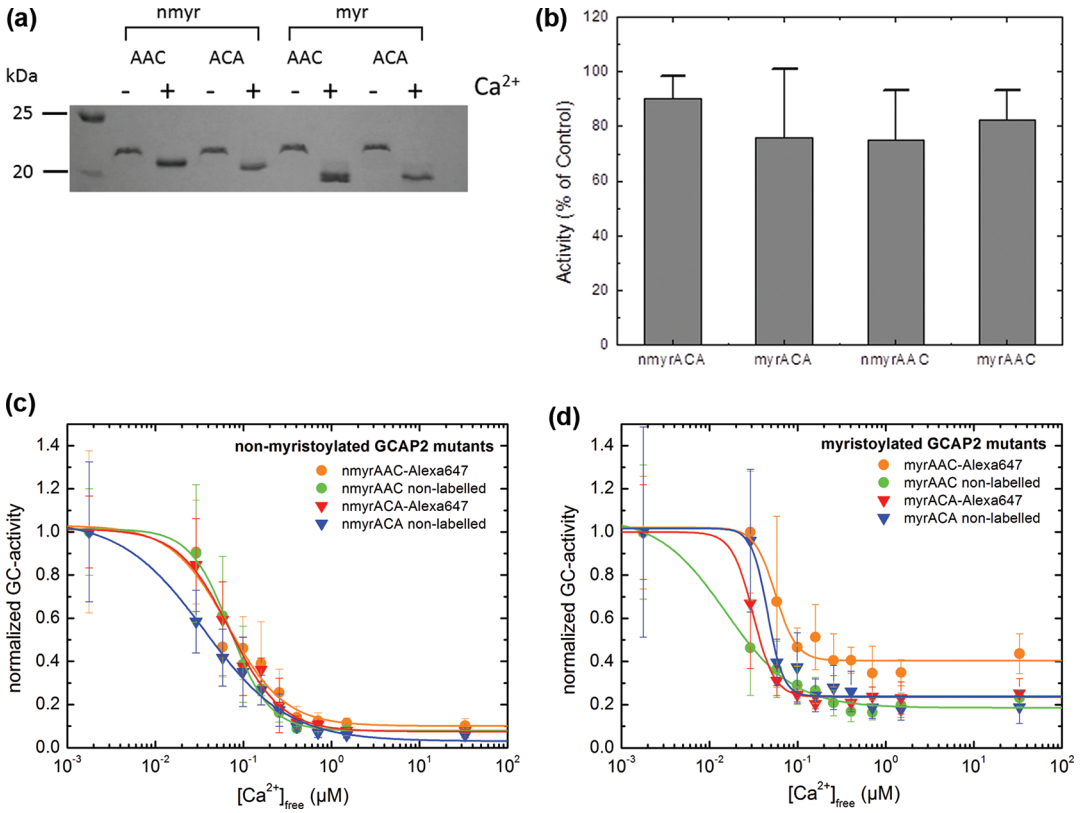

Figure 1. Biochemical characterization of GCAP2 mutants. (a) Ca^{2+}-dependent electrophoretic mobility shift of Alexa647-labeled GCAP2 mutants. One microgram of each purified GCAP2 form was analyzed by sodium dodecyl sulfate PAGE (12% acrylamide) in the absence (adding 2 mM EGTA, denoted by "−") or presence of Ca^{2+} (adding 2 mM $CaCl_2$, denoted by "+"). $MgCl_2$ was added at a concentration of 1 mM to increase the shift. Nonmyristoylated (nmyr) and myristoylated (myr) forms were compared. (b) Activation properties of GCAP2 mutants. Guanylate cyclase activity of bovine rod outer segment membranes was determined in the presence of nonlabeled and labeled GCAP2 mutants at low (3 nM) and high (33 μM) free Ca^{2+}, and the *x*-fold activation was determined for each. Values of *x*-fold activation obtained for the nonlabeled mutants were set to 100%, and the percentage of remaining activity of the labeled forms is shown in the figure (two independent sets of measurements). (c) Titration of Ca^{2+}-sensitive activation of ROS-GC by nonmyristoylated GCAP2 mutants as indicated in the legend. The following IC_{50} were determined (three data sets): 67 ± 16 nM (Alexa647-labeled AAC), 71 ± 4 nM (nonlabeled AAC), 70 ± 8 nM (Alexa647-labeled ACA), and 36 ± 5 nM (nonlabeled ACA). (d) Titration of Ca^{2+}-sensitive activation of ROS-GC by myristoylated GCAP2 mutants as indicated in the legend. IC_{50} values were 56 ± 6 nM (Alexa647-labeled AAC), 15 ± 5 nM (nonlabeled AAC), 31 ± 1 nM (Alexa647-labeled ACA), and 46 ± 6 nM (nonlabeled ACA). IC_{50} values of wildtype GCAP2 forms were in the same range below 100 nM free Ca^{2+} (data not shown).

when we tested the nonmyristoylated and the myristoylated GCAP2 forms (Figure 1c and d). Halfmaximal activation of ROS-GC (IC_{50} values) was observed between 30 and 80 nM free $[Ca^{2+}]$, the myristoylated unlabeled AAC mutant was even slightly more sensitive to Ca^{2+}. In general, the Ca^{2+}-sensitive activation profiles were in perfect agreement with our previous determinations of wildtype GCAP2 and the nonlabeled mutants ACA and AAC[30] and further confirmed that GCAP2 is responding to lower $[Ca^{2+}]$ than GCAP1.[23,31]

In summary, the introduction of the dye Alexa647 *via* coupling to an intrinsic cysteine left essential features of GCAP2 intact, providing useful tools for further fluorescence studies.

Fluorescence Lifetime Measurements. A series of fluorescence lifetime and rotational anisotropy measurements have been taken on Alexa647-labeled ACA and AAC GCAP2 mutants, both in myristoylated and nonmyristoylated form as well as in the presence and absence of free Ca^{2+}, *i.e.*, before or after adding the Ca^{2+}-chelator EGTA. Representative fluorescence decay curves of the myristoylated AAC mutant with EGTA (blue line) and without EGTA (red line) are shown in Figure 2a, together with the instrument response function (green line). The fluorescence signal decays on a typical time scale of a few nanoseconds and is well represented by a biexponential decay model (n = 2 in eq 5), as verified by the residuals plotted in Figure 2a. Similar agreement between experimental data and biexponential decay model is reached for all other fluorescence measurements. An overview of both fluorescence lifetime components (τ_1, τ_2) obtained from all investigated samples is given in Figure 2b. The fluorescence decay times of Alexa647 attached to the ACA mutant are in the range of 0.3−0.9 ns for τ_2 and range from 1.2 to 1.6 ns for τ_1. For the AAC mutants, we observe τ_2 values of 0.8−1.3 ns and τ_1 values of 1.9−2.2 ns. Clearly, the labeled AAC and ACA mutants can easily be distinguished by their two fluorescence decay time components.

In addition, the results summarized in Figure 2b reveal distinctly different decay kinetics of the labeled mutants at high and low $[Ca^{2+}]$. The arrows in Figure 2b indicate how the decay times τ_1 and τ_2 of a specific GCAP2 mutant are modified upon (i) decreasing the calcium concentration (+EGTA) and (ii) having the myristoyl group present (+myr) or not. In the case of ACA, an addition of EGTA to the buffer, *i.e.*, a removal of Ca^{2+} leads to an increase in both lifetime components irrespective of myristoylation. In this mutant, also the

dx.doi.org/10.1021/cb3000748 | *ACS Chem. Biol.* 2012, 7, 1006−1014

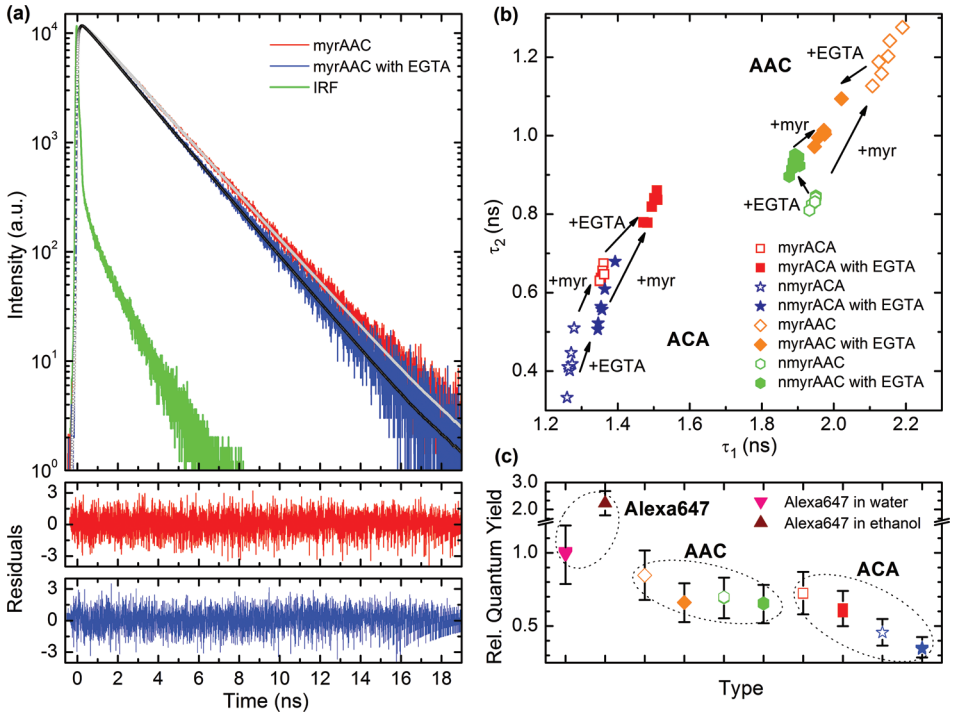

Figure 2. Fluorescence lifetime measurements of labeled GCAP2 mutants. (a) Representative time-resolved fluorescence decay of myristoylated AAC in the presence (red) and absence (blue) of calcium. Fits to a biexponential decay model with lifetime components τ_1 and τ_2 obtained by reconvolution with the instrument response function (green) are shown as white and black lines, respectively. The corresponding residuals are shown in the lower panels. (b) Summary of the fluorescence lifetime components extracted for all investigated samples. Results of 6 independent measurements are given for each sample. The arrows are guides to the eye indicating the change in lifetimes upon myristoylation or addition of EGTA, respectively. In this plot, AAC and ACA mutants are clearly distinguishable as two well-separated groups. Myristoylation results in an increase of $\tau_{1/2}$ irrespective of the type of mutant. (c) Relative fluorescence quantum yields of GCAP2 mutants, normalized to the yield of free Alexa647 in water. AAC mutants consistently show quantum yields larger than those of the corresponding ACA samples. Our results indicate an increase in quantum yield upon myristoylation, whereas the addition of EGTA decreases this yield.

attachment of the myristoyl group leads to an increase in both decay components, irrespective of EGTA addition.

In the nonmyristoylated AAC sample, a reduction in $[Ca^{2+}]$ by EGTA addition causes a decrease of the longer and an increase of the shorter decay time. In myristoylated AAC, however, removal of Ca^{2+} results in a decrease of both components. The effect of myristoylation on AAC is that both decay time components increase, which is more pronounced at high $[Ca^{2+}]$.

Relative fluorescence quantum yields, obtained using eq 6 and normalized to that of free Alexa647 dye in a water buffer, are depicted in Figure 2c. In general, the quantum yields show similar trends as the fluorescence decay times, even though the ACA and AAC mutants cannot be distinguished as clearly as from the lifetime measurements. For both mutants, an addition of EGTA leads to a decrease of the quantum yield, an effect that is more pronounced in ACA. Myristoylation, on the other hand, leads to an increase of the quantum yield. Quantum yield measurements on free Alexa647 dye in ethanol showed an increase by a factor of 2.2 compared to those in the more polar water buffer.

Fluorescence Anisotropy Measurements. Representative results of our fluorescence anisotropy measurements $r(t)$ are depicted in Figure 3a, showing the anisotropy decay of nonmyristoylated AAC in the presence and absence of Ca^{2+}. Two distinctly different decay times are discerned, a fast rotational correlation time ϕ_1 of several hundred ps and a very slow correlation time ϕ_2 of more than 10 ns. For all investigated samples, the $r(t)$ curves are well represented by a biexponential decay model (eq 8 with $n = 2$). The correlation times determined from all of our anisotropy measurements are summarized in Figure 3b.

It is evident that the rotational diffusion dynamics of the AAC and ACA mutants are distinctly different. For AAC, the fast component ϕ_1 lies in the range of 0.3−0.45 ns, whereas the slow component ϕ_2 varies between 20 and 100 ns. The effects of a variation in calcium concentration and of myristoylation on the rotational diffusion dynamics are clear. The removal of calcium increases both the ϕ_1 and ϕ_2 components, whereas myristoylation decreases both components significantly.

In the case of the ACA mutant, however, the component ϕ_2 is so slow (>100 ns) that it can no longer be extracted with certainty due to the much faster overall fluorescence decay in these samples. Here, we can just state that the slow rotational correlation of the ACA mutant amounts to more than 100 ns. The fast correlation time ϕ_1 lies in the range from 0.5 to 0.6 ns and increases significantly upon addition of Ca^{2+}, whereas the myristoylation effect is weak.

Discussion. Our results firmly indicate that site-specific labeling of the neuronal calcium sensor GCAP2 offers an interesting route toward probing conformational protein dynamics as a function of Ca^{2+}-binding and myristoylation. Labeling of GCAP2 mutants with the dye Alexa647 seems well suited for this purpose because essential features of GCAP2 function such as Ca^{2+}-induced conformational changes and regulation of guanylate cyclase activities were almost unaltered after labeling. In this study, we used fluorescence lifetime and

dx.doi.org/10.1021/cb3000748 | ACS Chem. Biol. 2012, 7, 1006−1014

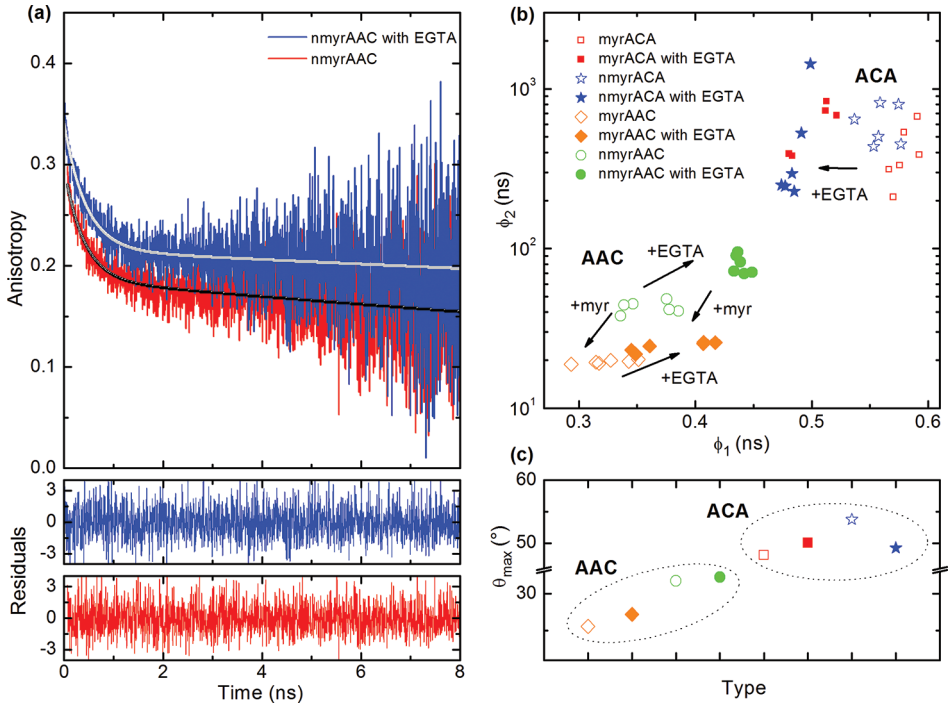

Figure 3. Fluorescence anisotropy measurements. (a) Fluorescence anisotropy decay of myristoylated AAC in the presence (red) and absence of calcium (blue) together with fits to a biexponential decay model with rotational correlation times Φ_1 and Φ_2 (black and white lines). The corresponding residuals are shown in the lower panels. (b) Summary of the fluorescence lifetime components extracted for all investigated samples. Again, the GCAP2 mutants can be separated into two distinct groups, with AAC showing rotational correlation times shorter than those for ACA. (c) Semicone angles θ_{max} derived from the "wobbling-in-a-cone" model for all investigated samples. Marked differences in θ_{max} for AAC and ACA mutants and variations in θ_{max} upon myristoylation and/or addition of calcium indicate the sensitivity of the rotational motion of the marker dye to changes in the protein conformation.

anisotropy measurements to investigate the changes in protein conformation in response to its microenvironment in solution.

For the interpretation of our results it is important that a previous systematic study of the fluorescence properties of Alexa647 in water and ethanol showed an increase in fluorescence lifetime in a more hydrophobic environment.[34] On the basis of these results we can draw some general conclusions from our measurements. Since the fluorescence decay of AAC is slower than that of the ACA mutant under all tested conditions, Alexa647 in position 131 senses a more hydrophobic environment than the dye in position 111. The presence of Ca^{2+} further increases the fluorescence lifetime, indicating that the dye is moving into a more hydrophobic environment, probably into a cleft inside of GCAP2. The opposite is observed for the ACA mutant, in which removal of Ca^{2+} increases the lifetime. Thus, the dye in position 111 is more strongly exposed to the polar solvent when the EF-hands in GCAP2 are occupied by Ca^{2+}.

Covalent attachment of the myristoyl group also causes an increase in decay time constants. This can be interpreted in two ways: first, the myristoyl group may stabilize a conformation in GCAP2 that facilitates a movement of residue 131 into a hydrophobic cleft. Second, the hydrophobicity of the myristoyl group may be sensed by the dye, because the dye is positioned in the vicinity of the myristoyl chain. A similar influence of the myristoyl group was also seen with the ACA mutant.

Solid-state ^2H NMR studies have shown that the myristoyl group of GCAP2 can insert into a lipid membrane that is present in the vicinity of the protein. Otherwise, the fatty acyl chain is expected to be buried into a hydrophobic protein pocket.[21,22] The contribution of the myristoyl group to the free energy of binding to lipids was determined to be only around −0.5 kJ/mol, indicating that the main driving force to interact with membranes must come from other, mostly hydrophobic amino acid side chains in GCAP2.[21] A further study on this topic concluded that the myristoyl group is in equilibrium between a membrane-inserted and an exposed state.[35] Thus, the myristoyl group in GCAP2 should be more flexible than in GCAP1, where it is buried in a hydrophobic cleft and does not move by changing $[Ca^{2+}]$.

The quantum yields reported in Figure 2c provide further support for our assumption that the dye interacts with either the polar solvent or the hydrophobic protein environment by modification of the protein−dye conjugate or the position of the dye in the protein. On the basis of our fluorescence lifetime and quantum yield measurements, we propose the phenomenological model depicted in Figure 4. Our data suggest that the myristoyl group is not completely exposed to the buffer solution but is instead situated on the surface of GCAP2 such that the solvent hydrophobicity can be sensed by the dye in positions 111 and 131 (see arrows connected with +myr in Figure 2b). When Ca^{2+} binds to the EF-hands, position 111 becomes more exposed to the polar solvent, whereas position 131 is moving into a more hydrophobic environment. In Figure 4b putative hydrophobic amino acids are highlighted that might be sensed by the dye. This movement is more pronounced when AAC is myristoylated. Nonmyristoylated AAC exhibits only a minor increase of the time constant τ_1 when Ca^{2+} is bound and a decrease in τ_2. Due to the position of the monitoring dye at cysteine 111 and 131, we propose a movement of the connecting α-helix[36] (Figure 4a). This piston-like movement is probably part of a concerted rearrangement of

dx.doi.org/10.1021/cb3000748 | ACS Chem. Biol. 2012, 7, 1006−1014

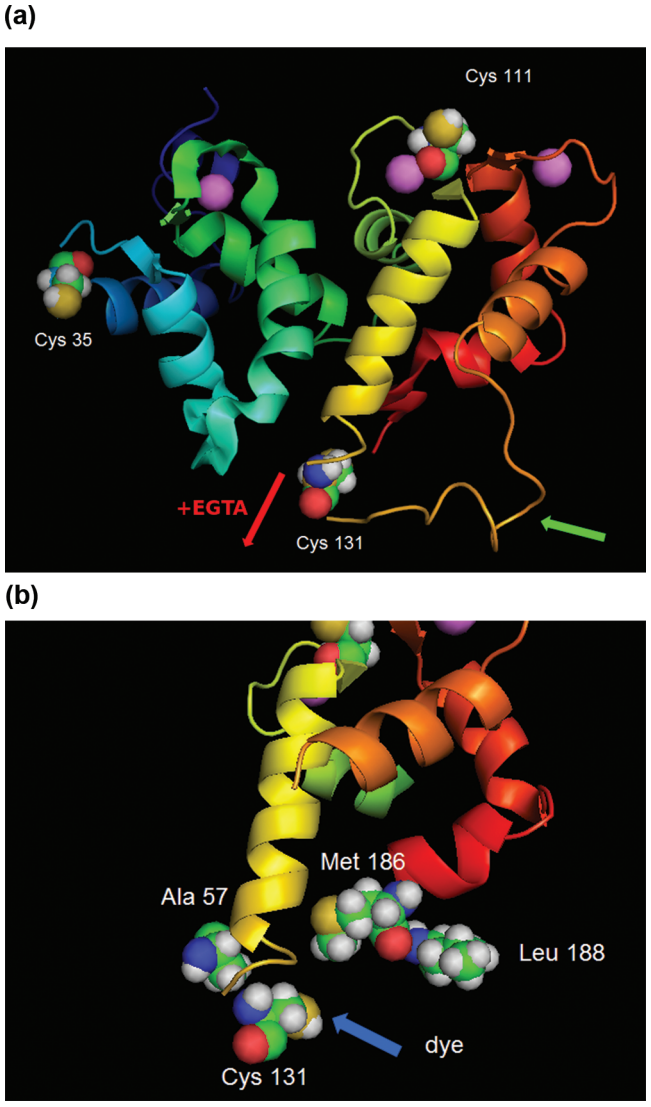

Figure 4. Structural model of Ca^{2+}-bound GCAP2 based on the NMR structure (PDB code: 1JBA). (a) Complete model of GCAP2 with the α-helix connecting cysteines 111 and 131 shown in yellow; cysteine residues are depicted in space-filled spheres. Movement of the α-helix when Ca^{2+} dissociates is indicated by the red arrow. The three functional EF-hands are coordinating each a Ca^{2+} ion (pink). The green arrow is pointing to the flexible loop region extending from cysteine 131. (b) Partial structure of GCAP2 as seen from a different angle to better visualize putative hydrophobic amino acid side chains in the vicinity of the covalently attached dye (position indicated by the blue arrow). Figures were created with pymol.

other regions in GCAP2 on Ca^{2+}-binding or dissociation. For example, the flexible loop region that extends from the cysteine residue at position 131 is exposed in Ca^{2+}-bound GCAP2 and more constrained in Ca^{2+}-free GCAP2.[37] This exposure as illustrated in Figure 4a could be the consequence of the upward movement of the connecting α-helix, which ultimately might be involved in controlling guanylate cyclase activity. Consistent with this assumption is that a critical region for controlling guanylate cyclase activity is located between phenylalanine at position 78 and aspartate at position 113 encompassing cysteine at position 111.[38] Although interaction of GCAP2 with guanylate cyclase occurs at the nonfunctional EF-hand 1,[39] we propose that the conformational change that transfers GCAP2 into the activating modus is mediated by the helix movement involving cysteine 111.

Additional evidence for such a putative model stems from our fluorescence anisotropy measurements, giving insight into the rotational dynamics of the dye/protein complex.[40] All of our measurements reveal biexponential decays with distinctly different fast (ϕ_1) and slow (ϕ_2) rotational correlation times in the range of a fraction of a ns and several tens of ns, respectively. With our experimental accuracy, the decay traces show no sign of a higher order multiexponential decay. It thus seems tempting to assign the fast and slow components to the rotational motion of the dye molecule bound to the protein and to the overall motion of the dye/protein complex, respectively, even though such a simplified interpretation should certainly be considered with some care.[40] The fact that $r(t)$ remains locked to more than 1/3 of its initial value, $r_0 = r(0)$, indicates that the ensemble-averaged correlation between the emission dipole moment vector at time t and the initial orientation of the absorption dipole moment vector is not completely lost and hence that the protein restricts the rotational motion to a certain confined geometry. Indeed, all our experimental results can be quantitatively described within a phenomenological "wobbling-in-a-cone" model,[41,42] in which the presence of the protein hinders the reorientational motion of the dye dipole and restricts it to a cone with finite semicone angle θ_{max}. Within this model, the rotational anisotropy $r(t)$ is given as

$$r(t) = r_0(1 - A_\infty)\, e^{-\left(\frac{1}{\phi_D}+\frac{1}{\phi_G}\right)t} + r_0 A_\infty\, e^{-t/\phi_G} \qquad (1)$$

Here, A_∞ is a parameter describing the finite correlation between emission and initial absorption dipole remaining after the dye dipoles are statistically distributed. r_0 denotes the initial value of the anisotropy, ϕ_D the reorientational correlation time of the dye molecule, and ϕ_G that of the dye/protein complex. The motional restriction parameter A_∞ is correlated to the semicone angle θ_{max} by

$$A_\infty = \left[\frac{1}{2}(1 + \cos\theta_{max})\cos\theta_{max}\right]^2 \qquad (2)$$

By comparing the anisotropy decay coefficients of eq 1 with those of eq 8 the semicone angle for each investigated sample can be determined to be

$$\theta_{max} = \cos^{-1}\left(\sqrt{2\left(\left(\frac{A_1}{A_2}+1\right)^{-1/2}+\frac{1}{8}\right)}-\frac{1}{2}\right) \qquad (3)$$

The motional restriction parameters and semicone angles deduced from our experiments are summarized in Table 2.

As seen from the graphical representation in Figure 3c, the semicone angles of the two mutants are distinctly different and amount to about 30° for AAC and to about 50° for ACA. This is indeed consistent with the schematic picture presented in Figure 4. The dye molecule attached to the cysteine in position 111 (ACA) is more strongly exposed to the solvent and hence its rotational motion is less restricted than that of the dye in the AAC mutant, giving rise to a significantly larger value of θ_{max} (Figure 3c).

The piston model in Figure 4 suggests that an increase in Ca^{2+} should move the dye molecule in the AAC mutant more deeply into a hydrophobic cleft in the inside of the GCAP2 protein, further confining its rotational motion. This is indeed

dx.doi.org/10.1021/cb3000748 | ACS Chem. Biol. 2012, 7, 1006–1014

Table 2. Calculated Values for the Degree of Motional Restriction (A_∞) and Semicone Angle θ_{max} of Alexa647 Attached to GCAP2 Mutants[a]

	A_∞ (θ_{max})	
	ACA	AAC
myr	0.31 (48.1°)	0.73 (25.6°)
+EGTA	0.28 (50.0°)	0.70 (27.2°)
nmyr	0.22 (53.8°)	0.62 (31.7°)
+EGTA	0.28 (49.2°)	0.61 (32.3°)

[a]The calculations are based on the "wobbling-in-a-cone" model eq 1 and describe the flexibility of the dye at the surface of the protein.

in qualitative agreement with the observed slight reduction in θ_{max} and ϕ_D. In ACA, the opposite effects should be seen. Whereas ϕ_D increases, θ_{max} shows a slight decrease for myristoylated ACA rather than an increase, indicating that certainly not all our observations can be explained by such a simplified mechanistic model. In both mutants, myristoylation results in a decrease of the maximum semicone angle, indicating a reduction in rotational flexibility of the attached dye molecules.

The overall time scale of the slow rotational correlation time ϕ_G of the dye/protein complex of few tens of ns agrees well with estimates based on the Stokes–Einstein–Debye equation for the correlation time:

$$\tau_c = \frac{4\pi r_{St}^3 \eta}{3k_B T} \quad (4)$$

Here k_BT is the Boltzmann factor, r_{St} the Stokes' radius, and η the viscosity of the solvent. For a Stokes' radius of r_{St} = 22 Å for monomers and r_{St} = 34 Å for dimers, based on measurements performed on GCAP1,[26] and the viscosity of water (η = 1 mNs/m^2 at 293.15 K) the rotational diffusion time is expected to be about 11 and 41 ns, respectively. All measured slow anisotropy decay components are of similar magnitude, supporting the assignment of ϕ_G to the rotational motion of the dye/protein complex. It is known that GCAP2, while existing in monomeric form in the presence of Ca^{2+}, undergoes reversible dimerization upon removal of Ca^{2+} (addition of EGTA).[37,43] One may hence expect a certain increase in ϕ_G upon decrease in [Ca^{2+}]. The experimental results reported in Figure 3, however, indicate much more pronounced variations in ϕ_G than expected based on Ca^{2+}-induced changes in the monomer/dimer equilibrium. One may ask whether and possibly to what extent homofluorescence resonance transfer (FRET),[44] *i.e.*, energy transfer between fluorophores in GCAP2 dimers, affects the anisotropy signals? Homo-FRET is known to result in bi- or multiexponential anisotropy decays similar to those in eq 1 with a fast decay reflecting the energy transfer time and slow decay governed by the rotational motion of the dimer complex. The fast decay is therefore mainly governed by the relative orientation of and the distance between the fluorophores. Our experimental data show comparatively large variations of more than 50% in ϕ_D upon myristoylation and/or Ca^{2+} addition, even though the relative orientation and distance between chromophores is likely to be only weakly affected. This makes it unlikely that homo-FRET has a significant influence on the measured anisotropy curves, even though minor contributions cannot be ruled out at the present stage. We also note that Ca^{2+}-free GCAP2 is present in a mixture of almost equal amounts of monomers and dimers.[37] If homo-FRET was important, this would lead to substantially different rotational anisotropy signals from monomers and dimers and hence to rather complicated multiexponential decays,[44] which are not observed experimentally. We take this as an additional indication, that homo-FRET is of minor importance for the anisotropy decay. Finally, since the cysteine mutation is unlikely to strongly affect the overall protein configuration and since the electrophoretic mobility of the mutants is similar to that of wildtype GCAP2 (Figure 1a), we presume that some of the variations in ϕ_G might be influenced by the finite accuracy of our anisotropy measurements, limited by the short fluorescence lifetime of the dye marker. These effects certainly deserve further study.

Summary and Conclusions. In summary, we have reported a time-resolved fluorescence study of different site-specifically labeled cysteine mutants of GCAP2. Our results show that labeling of such mutants with the fluorescent dye Alexa647 provides an interesting and flexible strategy for probing local conformational changes of the protein *via* their influence on the fluorescence dynamics of the dye marker. Specifically, we report distinct variations in fluorescence decay and rotational anisotropy dynamics when externally changing the Ca^{2+} concentration, upon myristoylation and upon variation of the position of the local dye marker. Our results suggest a mechanistic model for the Ca^{2+}-regulated protein motion in which saturation of GCAP2 with Ca^{2+} leads to a concerted movement of cysteines at position 111 and 131. The outgoing α-helix of EF-hand 3 is located between these two cysteines,[36] and we propose a piston-like up and down movement of this helix induced by Ca^{2+} binding or dissociation. An extension of our approach toward the site specific labeling of two cysteines with different dye markers may give insight into the vectorially correlated dye dynamics. Such experiments are currently underway in our laboratory.

METHODS

Expression and Purification of GCAP2, WT and Cysteine Mutants. Construction and expression of wildtype bovine GCAP2 and its cysteine mutants have been described in detail before.[30,33] Briefly, pET-11a vectors harboring the cDNA of GCAP2 mutants (two cysteines exchanged for alanine and one cysteine left resulting in mutants assigned as C35AA, AC111A and AAC131; for simplicity numbers are omitted in the text) were used for transformation of *E. coli* BL21-Codon Plus cells.[30,33] For the expression of myristoylated variants, *E. coli* cells were cotransformed with the plasmid pBB-131, harboring the gene for *N*-myristoyl-transferase from yeast *S. cerevisiae*. Expression of proteins was induced by the addition of isopropyl-β-D-thiogalactoside at final concentration of 1 mM. After 4 h of incubation at 37 °C bacteria were harvested by centrifugation (10 min at 5000*g*, 4 °C). Purification of GCAP2 variants from the cell pellet was achieved as described previously by a combination of anion exchange chromatography, ammonium sulfate precipitation, and size exclusion chromatography.[30] The protocol was modified for the myristoylated mutant AAC, since the protein was not completely pure after the size exclusion step and was therefore purified by an additional anion exchange step on a MonoQ 5/50 column (GE healthcare). This time, however, the chromatography was conducted in the absence of $CaCl_2$ (addition of 2 mM EGTA to the chromatography buffers as in ref 30). Purity of protein samples and Ca^{2+}-dependent electrophoretic mobilities were analyzed by sodium dodecyl sulfate PAGE as before.[11,26] Protein concentration was determined by a Coomassie Blue assay and concentration of purified GCAP2 samples was determined by UV-absorbance spectroscopy[23] at 280 nm using an extinction coefficient of 35210 M^{-1} cm^{-1}. The degree of myristoylation of GCAP2 variants was determined by reversed phase HPLC on a silica gel C18-column (VYDAC) as described before.[18]

dx.doi.org/10.1021/cb3000748 | *ACS Chem. Biol.* 2012, 7, 1006–1014

Fluorescence Labeling with Alexa647. Lyophilized GCAP2 mutants were dissolved in 10 mM Hepes-KOH pH 7.0 at a final concentration of 30−40 μM. Alexa647-maleimide (Molecular Probes) was added in 5-fold molar excess in a final volume of 0.4 mL. The reaction was allowed to proceed in a light-protected vial for 2−3 h and was terminated by addition of 2 mM dithiothreitol. Excess dye was removed by passing the reaction mixture over a NAP5 column (GE Healthcare), equilibrated in 125 mM NaCl, 25 mM Tris-HCl pH 7.4 (fluorescence buffer). If unreacted dye was still present after this treatment, it was removed by dialysis against the same buffer. The amount of bound dye was determined by recording the absorbance spectra of labeled GCAP2 mutants (0.4−0.5 μM) with a UV−vis spectrophotometer (SPECORD 205, Analytik Jena) in fluorescence buffer. The absorbance maximum at 650 nm was used to calculate the amount of attached dye employing a molar extinction coefficient of 265,000 M^{-1} cm^{-1}. The Coomassie Blue assay was employed for determination of the GCAP2 mutant concentration.

Guanylate Cyclase Assay. Reconstitution of purified and labeled GCAP2 mutants with membrane-bound photoreceptor guanylate cyclases was performed exactly as described earlier.[23] For this purpose membranes were prepared from bovine rod outer segment preparations as reported, which served as a source for membrane bound ROS-GCs.[23,33] The cyclase activities in the presence of wildtype and mutant GCAP2 were determined at 33 μM and 3 nM free [Ca^{2+}] resulting in a minimum GC activity (GC_{min}) at high 33 μM Ca^{2+} and a maximum (GC_{max}) at 3 nM Ca^{2+}. The *x*-fold activation is expressed as $x = (GC_{max} - GC_{min})/GC_{min}$. Values obtained with wildtype GCAP2 were set to 100% and compared with the activities in the presence of GCAP2 mutants. In order to test for the influence of dye attachment the labeled GCAP2 forms were compared with the corresponding nonlabeled forms. Furthermore, we determined the GC activities at intermediate free [Ca^{2+}] as previously described,[23,30,33] which allows a more precise comparison with the nonlabeled wildtype.

Fluorescence Lifetime Measurements. Fluorescence lifetime measurements have been performed by time-correlated single photon counting (TCSPC), using a pulsed diode laser (PicoQuant, PDL-800) operating at a repetition rate of 6 MHz and providing 50-ps pulses, centered at 656 nm and with an average power of a few μW. Vertically (0°) polarized laser pulses were weakly focused into a microcuvette using a f = 260 mm lens.

The emitted fluorescence light from the sample has been collected and focused onto an avalanche photodiode (ID Quantique 100) using a glass objective (Nikon, NA = 0.7). Lifetime measurements were performed under magic angle (54.7°) conditions to avoid any influence of fluorescence anisotropies. The collected decay curves were fitted to an exponential model by reconvolution:

$$I(t) = \int_{-\infty}^{t} IRF(t') \sum_{i=1}^{n} A_i \, e^{-\frac{t-t'}{\tau_i}} \, dt' \tag{5}$$

The parameter A_i denotes the amplitude of decay component i with decay time τ_i, and IRF(t) represents the instrument response function, which has been measured by use of scattered excitation light. The full width at half-maximum (fwhm) of the IRF was about 92 ps.

The fluorescence quantum yield QY was calculated on the basis of the integrated number of counts per lifetime measurement and the transmittance T of the sample compared to a reference quantum yield QY_R:

$$QY = \frac{\int I(t)\,dt}{\int I_R(t)\,dt}\left(\frac{1 - T_R}{1 - T}\right)QY_R \tag{6}$$

The quantum yield of Oxazine 1 in ethanol (QY_R = 0.11)[45] was used as reference. Excitation intensity and integration time have been kept constant for corresponding measurements of sample and reference, respectively.

Fluorescence Anisotropy. Fluorescence anisotropy measurements were performed by recording the fluorescence emission for two different detection polarizations, perpendicular ($I_\perp$) and parallel ($I_\parallel$) to the vertically polarized excitation light. The fluorescence anisotropy $r(t)$ is then deduced as

$$r(t) = \frac{I_\parallel(t) - G \cdot I_\perp(t)}{I_\parallel(t) + 2G \cdot I_\perp(t)} \tag{7}$$

The factor G was introduced to correct for the polarization anisotropy of our experimental setup. A factor of G = 1.05 was determined from calibration measurements on Oxazine 1. All anisotropy decay curves were fitted to the following model to determine the rotational correlation times of different samples.

$$r_{fit}(t) = \sum_{i=1}^{n} A_i \, e^{-\frac{t}{\phi_i}} \tag{8}$$

Here, A_i denotes the amplitude of the anisotropy decay component i and ϕ_i its correlation time.

AUTHOR INFORMATION

Corresponding Author

*E-mail: karl.w.koch@uni-oldenburg.de.

Notes

The authors declare no competing financial interest.

ACKNOWLEDGMENTS

This work was supported by grants from the Deutsche Forschungsgemeinschaft (KO 948/7-2, Li 580/8-1) and from the Korea Foundation for International Cooperation of Science & Technology (Global Research Laboratory project, K20815000003). We thank J. Gordon (Washington University School of Medicine, St. Louis, MO, USA) for kindly providing the plasmid vector for expression of yeast *N*-myristoyltransferase.

REFERENCES

(1) Pugh, E. N. Jr., and Lamb, T. D. (2000) Phototransduction in vertebrate rods and cones: molecular mechanisms of amplification, recovery and light adaptation. *Handb. Biol. Phys. 3*, 183−255.

(2) Luo, D. G., Xue, T., and Yau, K. W. (2008) How vision begins: an odyssey. *Proc. Natl. Acad. Sci. U.S.A. 105*, 9855−9862.

(3) Pugh, E. N. Jr., Nikonov, S., and Lamb, T. D. (1999) Molecular mechanisms of vertebrate photoreceptor light adaptation. *Curr. Opin. Neurobiol. 9*, 410−418.

(4) Makino, C. L., Wen, X. H., and Lem, J. (2003) Piecing together the timetable for visual transduction with transgenic animals. *Curr. Opin. Neurobiol. 13*, 404−412.

(5) Kaupp, U. B., and Seifert, R. (2002) Cyclic nucleotide-gated ion channels. *Physiol. Rev. 82*, 769−824.

(6) Yau, K. W., and Nakatani, K. (1985) Light-induced reduction of cytoplasmic free calcium in retinal rod outer segment. *Nature 313*, 579−582.

(7) Philippov, P. P., and Koch, K.-W., Eds. (2006) *Neuronal Calcium Sensor Proteins*, Nova Publishers, Hauppauge, NY.

(8) Palczewski, K., Polans, A. S., Baehr, W., and Ames, J. B. (2000) Ca^{2+}-binding proteins in the retina: structure, function, and the etiology of human visual diseases. *BioEssays 22*, 337−350.

(9) Palczewski, K., Subbaraya, I., Gorczyca, W. A., Helekar, B. S., Ruiz, C. C., Ohguro, H., Huang, J., Zhao, X., Crabb, J. W., Johnson, R. S., Walsh, K. A., Gray-Keller, M. P., Detwiller, P. B., and Baehr, W. (1994) Molecular cloning and characterization of retinal photoreceptor guanylyl cyclase-activating protein. *Neuron 13*, 395−404.

(10) Dizhoor, A. M., Olshevskaya, E. V., Henzel, W. J., Wong, S. C., Stults, J. I., Ankoudinova, I., and Hurley, J. B. (1995) Cloning,sequencing, and expression of a 24-kDa Ca2+-binding protein activating photoreceptor guanylyl cyclase. *J. Biol. Chem. 270*, 25200−25206.

(11) Frins, S., Bönigk, W., Müller, F., Kellner, R., and Koch, K.-W. (1996) Functional characterization of a guanylyl cyclase-activating protein from vertebrate rods. *J. Biol. Chem. 271*, 8022−8027.
(12) Zozulya, S., and Stryer, L. (1992) Calcium-myristoyl protein switch. *Proc. Natl. Acad. Sci. U.S.A. 89*, 11569−11573.
(13) Ames, J. B., Ishima, R., Tanaka, T., Gordon, J. I., Stryer, L., and Ikura, M. (1997) Molecular mechanics of calcium-myristoyl switches. *Nature 389*, 198−202.
(14) Ames, J. B., Porumb, T., Tanaka, T., Ikura, M., and Stryer, L. (1995) Amino-terminal myristoylation induces cooperative calcium binding to recoverin. *J. Biol. Chem. 270*, 4526−4533.
(15) Weiergräber, O. H., Senin, I. I., Philippov, P. P., Granzin, J., and Koch, K.-W. (2003) Impact of N-terminal myristoylation on the Ca^{2+}-dependent conformational transition in recoverin. *J. Biol. Chem. 278*, 22972−22979.
(16) Gensch, T., Komolov, K. E., Senin, I. I., Philippov, P. P., and Koch, K.-W. (2007) Ca^{2+}-dependent conformational changes in the neuronal Ca^{2+}-sensor recoverin probed by the fluorescent dye Alexa647. *Proteins 66*, 492−499.
(17) Olshevskaya, E. V., Hughes, R. E., Hurley, J. B., and Dizhoor, A. M. (1997) Calcium binding, but not a calcium-myristoyl switch, controls the ability of guanylyl cyclase-activating protein GCAP-2 to regulate photoreceptor guanylyl cyclase. *J. Biol. Chem. 272*, 14327−14333.
(18) Hwang, J. Y., and Koch, K.-W. (2002) Calcium- and myristoyl-dependent properties of guanylate cyclase-activating protein-1 and protein-2. *Biochemistry 41*, 13021−13028.
(19) Orban, T., Bereta, G., Miyagi, M., Wang, B., Chance, M. R., Sousa, M. C., and Palczewski, K. (2010) Conformation changes in guanylate cyclase-activating protein 1 induced by Ca^{2+} and N-terminal fatty acid acylation. *Structure 18*, 116−126.
(20) Stephen, R., Bereta, G., Golczak, M., Palczewski, K., and Sousa, M. C. (2007) Stabilizing function for myristoyl group revealed by the crystal structure of a neuronal calcium sensor, guanylate cyclase-activating protein 1. *Structure 15*, 1392−1402.
(21) Vogel, A., Schröder, T., Lange, C., and Huster, D. (2007) Characterization of the myristoyl lipid modification of membrane-bound GCAP-2 by ^2H solid-state NMR spectroscopy. *Biochim. Biophys. Acta 1768*, 3171−3181.
(22) Theisgen, S., Thomas, L., Schröder, T., Lange, C., Kovermann, M., Balbach, J., and Huster, D. (2011) The presence of membranes or micelles induces structural changes of the myristoylated guanylate-cyclase activating protein-2. *Eur. Biophys. J. 40*, 565−576.
(23) Hwang, J. Y., Lange, C., Helten, A., Höppner-Heitmann, D., Duda, T., Sharma, R. K., and Koch, K.-W. (2003) Regulatory modes of rod outer segment membrane guanylate cyclase differ in catalytic efficiency and Ca^{2+}-sensitivity. *Eur. J. Biochem. 270*, 3814−3821.
(24) Hughes, R. E., Brzovic, P. S., Dizhoor, A. M., Klevit, R. E., and Hurley, J. B. (1998) Ca^{2+}-dependent conformational changes in bovine GCAP-2. *Protein Sci. 7*, 2675−2680.
(25) Rudnicka-Nawrot, M., Surgucheva, I., Hulmes, J. D., Haeseleer, F., Sokal, I., Crabb, J. W., Baehr, W., and Palczewski, K. (1998) Changes in biological activity and folding of guanylate cyclase-activating protein 1 as a function of calcium. *Biochemistry 37*, 248−257.
(26) Hwang, J.-Y., Schlesinger, R., and Koch, K.-W. (2004) Irregular dimerization of guanylate cyclase-activating protein 1 mutants causes loss of target activation. *Eur. J. Biochem. 271*, 3785−3793.
(27) Sokal, I., Otto-Bruc, A. E., Surgucheva, I., Verlinde, C. L. M. J., Wang, C.-K., Baehr, W., and Palczewski, K. (1999) Conformational changes in guanylyl cyclase-activating protein 1 (GCAP1) and its tryptophan mutants as a function of calcium concentration. *J. Biol. Chem. 274*, 19829−29837.
(28) Hwang, J.-Y., Schlesinger, R., and Koch, K.-W. (2001) Calcium-dependent cysteine reactivities in the neuronal calcium sensor guanylate cyclase-activating protein 1. *FEBS Lett. 508*, 355−359.
(29) Sokal, I., Li, N., Klug, C. S., Filipek, S., Hubbell, W. L., Baehr, W., and Palczewski, K. (2001) Calcium-sensitive regions of GCAP1 as observed by chemical modifications, fluorescence, and EPR spectroscopies. *J. Biol. Chem. 276*, 43361−43373.
(30) Helten, A., and Koch, K.-W. (2007) Calcium-dependent conformational changes in guanylate cyclase-activating protein 2 monitored by cysteine accessibility. *Biochem. Biophys. Res. Commun. 356*, 687−692.
(31) Peshenko, I. V., and Dizhoor, A. M. (2006) Ca^{2+} and Mg^{2+} binding properties of GCAP-1. Evidence that Mg^{2+}-bound form is the physiological activator of photoreceptor guanylyl cyclase. *J. Biol. Chem. 281*, 23830−23841.
(32) Peshenko, I. V., and Dizhoor, A. M. (2007) Activation and inhibition of photoreceptor guanylyl cyclase by guanylyl cyclase activating protein 1 (GCAP-1): the functional role of Mg^{2+}/Ca^{2+} exchange in EF-hand domains. *J. Biol. Chem. 282*, 21645−21652.
(33) Helten, A., Säftel, W., and Koch, K.-W. (2007) Expression level and activity profile of membrane bound guanylate cyclase type 2 in rod outer segments. *J. Neurochem. 103*, 1439−1446.
(34) Buschmann, V., Weston, K. D., and Sauer, M. (2003) Spectroscopic study and evaluation of red-absorbing fluorescent dyes. *Bioconjugate Chem. 14*, 195−204.
(35) Schröder, T., Lilie, H., and Lange, C. (2011) The myristoylation of guanylate cyclase-activating protein-2 causes an increase in thermodynamic stability in the presence but not in the absence of Ca^2. *Protein Sci. 20*, 1155−1165.
(36) Ames, J. B., Dizhoor, A. M., Ikura, M., Palczewski, K., and Stryer, L. (1999) Three-dimensional structure of guanylyl cyclase activating protein-2, a calcium-sensitive modulator of photoreceptor guanylyl cyclase. *J. Biol. Chem. 274*, 19329−19337.
(37) Peshenko, I. V., Olshevskaya, E. V., and Dizhoor, A. M. (2004) Ca^{2+}-dependent conformational changes in guanylyl cyclase-activating protein 2 (GCAP-2) revealed by site-specific phosphorylation and partial proteolysis. *J. Biol. Chem. 279*, 50342−50349.
(38) Olshevskaya, E. V., Boikov, S., Ermilov, A., Krylov, D., Hurley, J. B., and Dizhoor, A. M. (1999) Mapping functional domains of the guanylate cyclase regulator protein, GCAP-2. *J. Biol. Chem. 274*, 10823−10832.
(39) Ermilov, A. N., Olshevskaya, E. V., and Dizhoor, A. M. (2001) Instead of binding calcium, one of the EF-hand structures in guanylyl cyclase activating protein-2 is required for targeting photoreceptor guanylyl cyclase. *J. Biol. Chem. 276*, 48143−48148.
(40) Hovius, R., Vallotton, P., Wohland, T., and Vogel, H. (2002) Fluorescence techniques: shedding light on ligand-receptor interactions. *Trends Pharmacol. Sci. 21*, 266−273.
(41) Schröder, G. F., Alexiev, U., and Grubmüller, H. (2005) Simulation of fluorescence anisotropy experiments: probing protein dynamics. *Biophys. J. 89*, 3757−3770.
(42) Kinosita, K., Kawato, S., and Ikegami, A. (1977) A theory of fluorescence polarization decay in membranes. *Biophys. J. 20*, 289−305.
(43) Olshevskaya, E. V., Ermilov, A. M., and Dizhoor, A. M. (1999) Dimerization of guanylyl cyclase-activating protein and a mechanism of photoreceptor guanylyl cyclase activation. *J. Biol. Chem. 274*, 255583−25587.
(44) Bader, A. N., Hoetzl, S., Hofman, E. G., Voortman, J., van Bergen en Henegouwen, P. M. P., van Meer, G, and Gerritsen, H. C. (2011) Homo-FRET imaging as a tool to quantify protein and lipid clustering. *ChemPhysChem 12*, 475−483.
(45) Sens, R., and Drexhage, K. H. (1981) Fluorescence quantum yield of oxazine and carbazine laser dyes. *J. Lumin. 24/25*, 709−712.